Mechanical Tomography of Human Corneocytes with a Nanoneedle

James D. Beard[1], Richard H. Guy[2], and Sergey N. Gordeev[1,3]

[1]Department of Physics and [2]Department of Pharmacy & Pharmacology

University of Bath, Claverton Down, Bath, BA2 7AY, U.K.

[3]Corresponding author: Department of Physics, University of Bath, Claverton Down, Bath, BA2 7AY, U.K. Email: s.gordeev@bath.ac.uk. Tel. (Fax) +44-1225-385154 (-386110)

Short title: Mechanical tomography of skin cells

Abbreviations: AFM = atomic force microscopy. SC = stratum corneum. Z = vertical piezo-displacement of AFM probe.

Abstract

Atomic Force Microscopy (AFM) can image biological samples and characterise their mechanical properties. However, the low aspect ratio of standard AFM probes typically limits these measurements to surface properties. Here, the intracellular mechanical behaviour of human corneocytes is determined using "nanoneedle" AFM probes. The method evaluates the forces experienced by a nanoneedle as it is pushed into and then retracted from the cell. Indentation loops yield the stiffness profile and information on the elastic and nonelastic mechanical properties at a specific depth below the surface of the corneocytes. A clear difference between the softer ~50 nm-thick external layer and the more rigid internal structure of corneocytes is apparent, consistent with current understanding of the structure of these cells. There are also significant variations in the mechanical properties of corneocytes from different volunteers. The small diameter of the nanoneedle allows this “mechanical tomography” to be performed with high spatial resolution, potentially offering an opportunity to detect biomechanical changes in corneocytes due (for example) to environmental factors, aging or dermatological pathologies.

Introduction

Mammalian skin is an impressive piece of bioengineering that acts as an interface with the external environment and as a barrier not only to the penetration of potentially harmful materials but also, and most significantly, to the loss of tissue water (Elias, 2005; Madison, 2003; Proksch et al., 2008). The latter objective is accomplished by the thin (10-20 μm on average) outer layer of the epidermis, the stratum corneum (SC) (Cork et al., 2009). Because the maintenance of barrier homeostasis is an essential requirement, the SC must be flexible and must be able to adapt to body movement without rupturing. The mechanics of how this is possible are unknown and a detailed investigation of the physical properties of the SC (elasticity, viscoelasticity, deformation) has not been performed. That these properties may be expected to change significantly from the base of the SC to the skin surface is evident from the very steep hydration gradient across the membrane (Kalia et al., 1996); indeed, it is well-known that xerotic skin is more fragile than that which retains a normal level of moisturisation (Rawlings and Harding, 2004; Ghadially et al., 1995).

Atomic force microscopy (AFM) has been used previously to probe the mechanical properties of the SC (Kasibuchi et al., 2002; Yuan and Verma, 2006; Gorzelanny et al., 2006; Fung et al., 2010). However, these measurements have been made either on entire, isolated membranes, or on individual corneocytes that had been aggressively separated using organic solvent, resulting in significant variability in the parameters observed (Richter et al., 2001). Similarly, the elastic properties of intact stratum corneum varied considerably depending on the size of AFM probe employed, suggesting a significant difference between global mechanical properties (on the scale of >10 μm) and nanoscale, local properties (over distances of <100 nm) (Yuan and Verma, 2006). Consequently, the detailed mechanical behaviour of corneocyte monolayers, and that of specific intracellular or surface structures, has not been characterised.

A common application of AFM uses indentation to study mechanics at the nanoscale (Weisenhorn et al., 1993; Radmacher, 1997). Different modifications of this technique, covering a wide force range from 10^{-12} to 10^{-5} N, have been used to measure the structure-property relationships of both technical materials and biological tissues. However, the pyramidal shape and low aspect ratio of standard AFM probes means that mechanical properties deep inside the cell cannot be determined, and limits the method to the evaluation of surface properties. There have been some attempts to use standard, pyramidal AFM probes to estimate the stiffness of cell structures buried beneath the indentation spot (Fuhrmann et al., 2011; Roduit et al., 2009) using the method of 'AFM stiffness nanotomography', and distinct differences between the mechanical properties of the ‘normal’ cell lines considered and the unusual 'crumbling' behaviour of cancerous cells have been demonstrated (Fuhrmann et al., 2011). However, any quantitative analysis of the 'force-displacement' curves obtained with standard AFM probes for deep indentations quickly becomes quite complicated as cells often show complex, nonlinear, viscoelastic behaviour and are highly heterogeneous both structurally and morphologically (Fletcher & Mullins, 2010). Also, the accuracy of estimations of internal structure stiffness falls off dramatically with increasing depth into the cell.

Recently, high aspect ratio structures (sometimes called “nanoneedles”) have been shown to penetrate biological cells to large depths, enabling, for example, manipulation of internal structures and microinjection of materials such as DNA (Han et al., 2005; Obataya et al., 2005; Patil et al., 2004; Vakarelski et al., 2007). A major advantage of these nanostructures is their ability to enter the cell without causing damage to its overall structure and thereby avoiding disruption of cell function. However, nanoneedles have not yet been used either to elucidate the mechanical properties of skin cells and or to study, at nanoscale resolution, their intracellular structures *in situ*. It is hypothesised that a clearer understanding of differences in the mechanical properties of normal versus ageing or diseased SC, and their relationship to

the quality of the membrane and to mechanical rupture, may ultimately lead to new therapeutic and/or diagnostic interventions to safeguard barrier function.

Results and Discussion

"Nanoneedles" with lengths of ~500 nm, and diameters from 30 to 80 nm, were created on the apex of standard AFM probes (Beard and Gordeev, 2011). The resulting structures were principally composed of amorphous carbon and had an approximately cylindrical shaft with a hemispherical apex (**Figure 1a**). Such nanoneedles are mechanically robust, survive large mechanical deformations without breaking, and recover elastically for deformations of up to 60% of their length.

Nanoindentation experiments were performed on corneocytes isolated from human stratum corneum (SC) using a simple adhesive stripping process. Corneocytes are flat, plate-like cells, typically ~0.5 μm thick and 10-30 μm across; they lack nuclei or organelles and are composed of a cross-linked protein envelope surrounding an internal matrix composed primarily of keratin filaments. **Figure 1b** (courtesy of L. Norlén, personal communication) shows a high-magnification image of part of a corneocyte from human SC; the latter is often characterised as a structure of corneocyte 'bricks' separated by well-organised lamellae of intercellular lipids (the 'mortar') (Al-Amoudi et al., 2005; Harding, 2004). The cornified envelopes of the cells appear as darker zones at the interface between the intercellular lipids and the intracellular keratin matrix of the corneocytes; as illustrated in **Figure 1b**, the thickness of the cornified envelope is variable, both within and between cells, ranging from 20 to more than 50 nm.

Figure 1c schematically illustrates the progressive penetration of nanoneedles into the corneocytes as performed in this work. Initially, the nanoneedle probe interrogates the

mechanical properties of the cell's lipid-protein envelope. With increasing applied force, the probe breaks through the envelope deeper into the cell and can then measure the mechanical properties of the internal matrix of keratin filaments and intracellular structures.

The AFM oscillation mode (or 'tapping-mode') images in **Figures 2a** and **2b** compare the corneocyte surface structure immediately before and after indentation using a nanoneedle probe of 40 nm diameter. The indent creates a small pore in the corneocyte surface without damage to the cell's overall structure. **Figure 2c** shows this more clearly and compares cross-sectional profiles along the same line on the cell surface before and after the indentation (**Figures 2a** and **2b**). The affected area is ~200 nm in diameter. Because of the nature of the corneocytes, the pore preserves its shape during nanoindentation, and does not seal over the time-frame involved. This simplifies the analysis of these results, as it is not necessary to take into account any dynamic changes in cell organisation.

Figure 3a gives examples of loading curves recorded during AFM indentation with a nanoneedle of 75 nm in diameter for several corneocytes from the same volunteer (aged 25 years). **Figure 3b** shows a set of loading curves for another volunteer (also 25 years old) obtained using a nanoneedle of similar diameter for four indents reaching different depths. The force (F), experienced by the nanoneedle when it is pushed into the cell, is proportional to the cantilever's deflection (D) and can be calculated as $F = k \bullet D$, where k is the cantilever spring constant (35 N/m in this case). It follows that the curves in these figures indicate both the deflection and the force as a function of the vertical piezo-displacement (ΔZ) of the AFM probe relative to the corneocyte surface. The cantilever deflection is significantly smaller than its vertical displacement, reflecting the choice of comparatively rigid AFM probes with k = 30-80 N/m for these experiments. The vertical position (h) of the nanoneedle tip with respect to the corneocyte surface, and hence the cell's deformation (indentation depth) produced by the nanoneedle, are equal to the vertical position of the cantilever base minus its deflection

(i.e., $h = [\Delta Z - D]$), and is mostly determined by ΔZ. The measured curves differ between separate indents corresponding most likely to variations in the structures encountered by the nanoneedle probe as it penetrated the cell. Near the surface, the mechanical inhomogeneity of the corneocyte could possibly be due to the probe coming into contact with desmosomal structures, the 'rivets' holding adjacent corneocyte layers together prior to their degradation in the upper SC and ultimate desquamation from the skin (Harding, 2004). It seems not unlikely that the cell surface mechanical properties on, or in the vicinity of, a desmosome may be different. Deeper in the cells, the observed variations are perhaps due to the nanoneedle encountering the protein filaggrin at different stages of its breakdown into 'natural moisturising factor' (Harding, 2004).

The loading curves have a common trend. When the probe is pushed into the cell, the resistance experienced by the nanoneedle increases (for Z > 40-80 nm in **Figure 3**). Given the general corneocyte structure (as illustrated in **Figure 1b**), the observed increase in the force gradient is attributed to the start of the interaction of the nanoneedle with the stiffer cell interior. The thickness of the surface layer incorporating the protein envelope varies significantly between cells and between individuals (**Figure 1b**) and this was observed in these experiments too.

The inset in **Figure 3b** illustrates this point with data, obtained with the same nanoneedle, showing the indentation of corneocytes from two volunteers aged 25 and 54 years. For the older volunteer, the abrupt increase in cell stiffness occurs at a depth of 32 nm, whereas the corresponding value for the younger individual is 43 nm. It is also clear from the shape of the loading curves that the force required to penetrate the corneocyte to the same depth is greater for the older volunteer. While these results are consistent with the skin thinning and becoming more brittle with increasing age, the significance of the difference seen cannot be assessed until many more subjects in different age groups have been studied.

The shape of the loading curves at low ΔZ values reflects the forces experienced by the nanoneedle as it penetrates through the surface layer; an example in **Figure 4a** exhibits a clear maximum, similar to that observed when AFM probes have penetrated through the plasma membrane of living cells (Fuhrmann et al., 2011; Obataya et al., 2005). However, in that case, the penetration force was much smaller (~1 nN) compared to that (~100 nN) for corneocytes. This makes sense given the presence of the cornified envelope. The exterior of the skin cell is also more brittle than the plasma membrane of living cells and, as shown below, cannot sustain large deformations. Thus, the behaviour shown in **Figure 4a** most probably reflects penetration through the external lipid-protein layer at the corneocyte surface to the mechanically softer material beneath. The force starts to increase when the nanoneedle hits the internal keratin structure of the cell (for $Z > 290$ nm, corresponding to $\Delta Z > 50$ nm in **Figure 4a**).

More typically, loading curves do not show such a maximum corresponding to the surface layer; rather, a decrease in the gradient is observed for depths between 10 and 40 nm (see **Figure 3b** inset). This indicates that the local stiffness of the surface layer does not vary significantly until the internal structure is reached. Taking the force at $\Delta Z = 50$ nm as an estimation of that required to penetrate the external surface layer, the histogram inset in **Figure 3a** was derived from the loading curves, some examples of which are shown in the main panel for the subject in question. The penetration forces ranged from 90 to 220 nN (average = 147 nN). For four subjects of similar ages (19-28 years), the overall spread of the penetration force was 30 to 260 nN.

Loading curves contain detailed information about the forces experienced by the nanoneedle as it is pushed into the cell, but do not reveal whether the cell was deformed elastically or inelastically. This information can be obtained from unloading curves, when the nanoneedle is pulled out of the cell (see **Figure 4a**). First, the AFM detection system is

calibrated by pressing the probe against an "underformable" sample, for which the cantilever deflection equals the vertical piezo-displacement of the AFM probe. Here, the calibration was performed on a silicon wafer, which is essentially underformable compared to the corneocyte. Subsequently, a full indentation loop was measured on a corneocyte with the same AFM probe, and the difference in *Z* between sample and calibration provides the overall deformation of the cell for different deflections. In the case shown in **Figure 4a**, the start of the unloading curve, practically speaking, coincides with the terminal part of the loading curve, implying that, in this area, the cell recovery was mainly elastic. However, when the nanoneedle is pulled out further, a hysteresis was apparent and a small upward force was required (negative overshoot in **Figure 4a**) to remove the nanoneedle from the cell. The size of the hysteresis at zero deflection corresponds to the inelastic deformation depth; i.e., to the depth of the hole made by the nanoneedle in the corneocyte. The difference between the maximum overall deformation and the 'inelastic deformation' gives an estimation of the elastic recovery of the cell.

Such measurements of full indentation loops corresponding to different ranges of applied forces enabled information to be obtained about the elastic limit of the corneocyte surface and subsequently about inelastic processes within the cell. Nanoneedles of two different diameters, 40 and 75 nm (see inset to **Figure 4c**) were used. Typical examples of loading curve loops are presented in the inset to **Figure 4b** and show that the thicker needle experiences larger forces during penetration into the cell. The main panel of **Figure 4b** shows the residual inelastic deformation of the corneocyte cells as a function of the maximum applied indentation force for indents with the two needles. Indentation with a thinner diameter needle results in greater inelastic deformation for smaller forces. However, all the curves display a similar trend, with a rapid increase in deformation at a depth of 100-200 nm, followed by a decrease in the rate of penetration as the force increases further. **Figure 4c** presents the same data scaled to the diameter of the nanoneedles and shows that there is only

elastic deformation at very low force-diameter ratios (below 2 N/m) followed by the onset of inelastic deformation at higher values. This onset likely corresponds to the elastic limit of the corneocyte surface layer. With increasing force, a further rapid increase in inelastic deformation occurs at ~10 N/m, possibly due to the rapid yielding of the internal keratin filament structure as it is deformed by the nanoneedle.

This scaling of the data with needle diameter probably indicates that breaking occurs in the region of maximum strain at the edges of the needle tip; the damage to the sample is concentrated around the circumference of the needle tip (which is proportional to its diameter). The similarity between the data obtained using nanoneedles of different diameters would suggest that the observed results reflect the properties of the corneocytes themselves rather than the characteristics of the nanoneedle probe.

These results permit an informed discussion of the origin of the measured forces. When the nanoneedle is pushed into the cell, it can experience (at least) elastic, plastic, viscous, adhesive and frictional (due to friction of the nanoneedle sidewalls within the pore) forces. During unloading, the situation is simpler, because no plastic deformation occurs (Oliver and Pharr, 1992). Viscous forces may affect the dynamics of this process but they can be decreased by reducing the speed of nanoneedle withdrawal (and they can also be taken into account in model calculations) (Oyen and Cook, 2003; Oyen and Ko, 2007). The joint effect of adhesive and frictional forces can be estimated from the negative part of full unloading loops where the magnitude of the cantilever displacement indicates the force required to withdraw the nanoneedle from the pore. As seen in **Figure 4a**, this 'negative overshoot' was usually small compared to the positive part of the indentation loops, indicating that friction was not a dominant force in the measurements reported here.

For quantitative analysis of nanoindentation curves, a number of models have been developed (Oyen and Cook, 2009). These are usually applied to unloading curves, because no

plastic deformation occurs during retraction and therefore the quantitative analysis is simpler. The Oliver-Pharr model (Oliver and Pharr, 1992), developed for plastic-elastic materials, is often applied to indentation data on both biological and non-biological samples, and extracts the elastic modulus from the slope of the force-deformation curve during retraction of the indenter. For a cylindrical indenter, the model suggests that elastic deformation is linear with respect to both the applied indentation force and the nano-indenter diameter. The local "reduced elastic modulus" (*E'*), at the depth to which the needle penetrates at the peak loading force, can be calculated from the initial slope (*dF/dh*) of the unloading curve, at the point of maximum penetration, from the relationship (Oliver and Pharr, 1992): $dF/dh = 2E'(A/\pi)^{1/2}$, where A is the projected contact area of the nanoneedle tip during indentation. The reduced elastic modulus is given by $E' = E/(1-\nu^2)$, where E is the Young's modulus and ν is the Poisson ratio of the sample material.

For classical indenters having a pyramidal shape (Oliver and Pharr, 1992), it is essential to measure the initial slope of the unloading curve because the area of contact of the indenter with the sample may vary significantly during retraction. However, for cylindrical indenters, the contact area is constant, the unloading curve is linear, and the slope can be taken from the central part of the curve. This facility is essential if the medium has some viscoelasticity because such an effect is most prominent at the region of the greatest indentation force and the Oliver-Pharr model does not take this into account. Thus, to reduce the impact of viscoelastic effects on the results presented here, analysis of the unloading curves was repeated, taking the average slope of the central part of these profiles (between 25 and 75%) and neglecting, therefore, the region of greatest indentation force and the point at which the indentation force decreases to zero.

The indentation data were also analysed using a model incorporating elastic, plastic and viscoelastic effects (Oyen and Cook, 2003). This approach assumes a linear sum of viscous

and elastic contributions to the deformation of a sample, and has previously been used to model the behaviour of biomaterials such as bone (Oyen and Ko, 2007).

Determination of the reduced elastic modulus using the two models, as a function of penetration depth for the same subject, is illustrated in **Figure 5a**; the different approaches give qualitatively the same dependence. **Figure 5b** shows the elastic moduli determined using the Oliver-Pharr method for different depths of penetration into corneocytes from 4 "young" (19-28 years old) subjects. The same trend is seen for all samples; i.e., a smaller elastic modulus near the cell surface and then, as the indentation depth was increased above ~50 nm, an increase in the value from about 100 to 500 MPa.

This analysis agrees with the two-layer interpretation of the shape of the force curves, and corresponds to the known structure of the corneocyte: that is, an external lipid-protein envelope (the softer, outer layer) surrounding a stiffer, internal matrix of keratin filament bundles. The value of ~100 MPa calculated for small indentation depths is similar to the surface elastic modulus of corneocytes determined by using indentation with standard AFM probes (Gaikwad et al., 2010). A significant scatter of results for depths above 100 nm, which can even be seen in data from the same volunteer, might possibly be attributed to local structural variations within corneocytes (perhaps due, as suggested above, to the presence of filaggrin at different stages in its degradation). It also should be noted that, even for the same volunteer, each experimental point corresponds to a different site on either the same cell or to a different cell; thus, any spatial variations in mechanical properties of such cells can contribute to the scatter in the experimental results.

It is important to emphasise that, while the results for elastic moduli within corneocytes presented in **Figure 5** are in qualitative agreement with the current understanding of the structure of these cells, the accuracy of the calculated values is difficult to estimate because both indentation models used were originally derived for homogeneous media. Nonetheless,

the models should still give reasonable values for samples consisting of two layers with drastically different elastic moduli (which more or less corresponds to the situation described here). Computer simulations based on a thorough analysis of both the loading and unloading curves should give a detailed picture of the mechanical properties for more complex cases (Dao et al., 2001; Tai et al., 2007).

In conclusion, this paper presents measurements of the mechanical properties of the internal structure of corneocytes, and shows that a nanoneedle can create a "tomography" profile of cell stiffness over a range of depths below the surface. The technique can map structural properties of cells with high spatial resolution, extending AFM measurements into three dimensions and thereby expanding its potential application in physiology and pharmacology at the nanoscale. In particular, this method allows nanoprobe penetration through the cell envelope to be detected and the elastic properties of intracellular structures to be determined. Loading curves give mostly information about stiffness of the cell material while unloading curves report on its elastic reaction (recovery). Applying existing indentation models to the unloading curves, the elastic modulus of the internal keratin structures of the corneocyte has been estimated for the first time since, until now, this cellular domain has not been accessible for *in situ* mechanical measurement. The results also provide support for the potential application of the nanoindentation technique to detect mechanical changes in cell structure, including those that are disease-related. Equally, in skin-care research, the technique may prove useful in the evaluation of clinical treatments or moisturisation, for example, or in assessing response to, and recovery from, ultraviolet light exposure from the sun.

Experimental Section

Fabrication of Nanoneedle Probes was performed as previously reported using Electron Beam Induced Deposition (EBID) with a Hitachi S-4300 SE SEM system equipped with a RAITH nanolithography system (Beard and Gordeev, 2011). A beam current of

approximately 100 pA and an accelerating voltage of 20 kV were used to grow nanoneedles. It should be pointed out that EBID-manufactured nanoneedles are now commercially available (e.g. EBD2-100 probes from Nanotools GmbH) and are suggested to have similar properties to multiwall carbon nanotube probes.

Corneocyte Preparation. Corneocytes were obtained from healthy human volunteers, four aged between 19 and 28 years and a fifth aged 54 years. Informed consent was obtained from all subjects before corneocyte removal. The procedure involved first delineating a 1 cm^2 area on the subject's forearm with standard surgical tape and measuring transepidermal water loss (TEWL) on this initially unperturbed skin site (Aquaflux, Biox Systems, Ltd., London, UK). Layers of corneocytes were then removed by stripping the stratum corneum using hair removal wax melted at 60°C on glass slides. TEWL was measured after each stripping to permit the thickness of stratum corneum removed to be determined and to ensure that the level of barrier disruption did not exceed 80% of the maximum possible (Kalia et al., 1996; Kalia et al., 2000). Removal of corneocytes using wax was employed because the relatively rigid substrate, once the wax had hardened, securely held the cells in place for mechanical testing.

AFM Imaging and Indentation Experiments were performed in air using an AFM operated in Tapping Mode (Veeco IIIa Multimode, Veeco Inc., USA). Nanoneedles fabricated by EBID on standard, commercially available Tapping Mode AFM probes (Budget Sensors, nominal spring constant ~40 N/m, resonance frequency ~300 KHz) were used for both imaging and indentation experiments. Spring constants for each AFM probe were calibrated based on resonant frequency and quality factor measurements (Sader et al., 1999; Sader, 1998) carried out using the AFM system, and the cantilever dimensions measured using SEM. The accuracy of this method is estimated to be ~20% of the calculated spring constant based on uncertainties in the SEM and AFM measurements of the cantilever. Pseudo-3D AFM

images and profile data were plotted using the WSxM software from Nanotec Electronica S.L. (Horcas et al., 2007).

Acknowledgements

We thank Dr. Lars Norlén of the Karolinska Institute, Sweden, for the images in **Figure 1b**.

Conflict of interest

The authors report no conflicts of interest.

References

Al-Amoudi A, Dubochet J, Norlén L (2005) Nanostructure of the epidermal extracellular space as observed by cryo-electron microscopy of vitreous sections of human skin. *J. Invest. Dermatol.* 124: 764-777.

Beard JD, Gordeev, SN (2011) Fabrication and buckling dynamics of nanoneedle AFM probes. *Nanotechnology* 22**:** 175303.

Cork MJ, Danby SG, Vasilopoulos Y, Hadgraft J, Lane ME, Moustafa M, Guy RH, Macgowan AL, Tazi-Ahnini R, Ward SJ (2009) Epidermal barrier dysfunction in atopic dermatitis. *J. Invest. Dermatol.* 129: 1892-1908.

Dao M, Chollacoop N, Van Vliet KJ *et al*. (2001) Computational modeling of the forward and reverse problems in instrumented sharp indentation. *Acta Mater.* 49: 3899–3918.

Elias PM (2005) Stratum corneum defensive functions: an integrated view. *J. Invest. Dermatol.* 125: 183-200.

Fletcher DA, Mullins RD (2010) Cell mechanics and the cytoskeleton, *Nature* 463: 485-492.

Fuhrmann A, Staunton JR, Nandakumar V *et al.* (2011) AFM stiffness nanotomography of normal, metaplastic and dysplastic human esophagal cells, *Phys. Biol.* 8: 015007.

Fung CK, Seiffert-Sinha K, Lai KW *et al.* (2010) Investigation of human keratinocyte cell adhesion using atomic force microscopy. *Nanomedicine* 6: 191-200.

Gaikwad R, Vasilyev S, Datta S *et al.* (2010) Atomic force microscopy characterization of corneocytes: effect of moisturizer on their topology, rigidity, and friction. *Skin Res. Technol.* 16**:** 275-282.

Ghadially R, Brown BE, Sequeira-Martin SM *et al.* (1995) The aged epidermal permeability barrier. Structural, functional, and lipid biochemical abnormalities in humans and a senescent murine model. *J. Clin. Invest.* 95: 2281-2290.

Gorzelanny C, Goerge T, Schnaeker EM *et al.* (2006) Atomic force microscopy as an innovative tool for nanoanalysis of native stratum corneum. *Exp. Dermatol.* 15: 387-391.

Han S, Nakamura C, Obataya I *et al.* (2005) A molecular delivery system using AFM and nanoneedle. *Biosens. Biotechnol.* 20: 2120-2125.

Harding, CR (2004) The stratum corneum: structure and function on health and disease. *Dermatologic Therapy* 17: 6-15.

Horcas I, Fernández R, Gómez-Rodríguez JM *et al.* (2007) WSXM: a software for scanning probe microscopy and a tool for nanotechnology. *Rev Sci Instrum* 78: 013705.

Kalia YN, Alberti I, Sekkat N *et al.* (2000) Normalization of stratum corneum barrier function and transepidermal water loss in vivo. *Pharm. Res.* 17: 1148-1150.

Kalia YN, Pirot F, Guy RH (1996) Homogeneous transport in a heterogeneous membrane: water diffusion across human stratum corneum in vivo. *Biophys J.* 71**:** 2692-2700.

Kashibuchi N, Hirai Y, O'Goshi K *et al.* (2002) Three-dimensional analyses of individual corneocytes with atomic force microscope: morphological changes related to age, location and to the pathologic skin conditions. *Skin Res. Technol.* 8: 203-211.

Madison KC (2003) Barrier function of the skin: "la raison d'être" of the epidermis. *J. Invest. Dermatol.* 121: 231-242.

Obataya I, Nakamura C, Han S *et al.* (2005) Nanoscale operation of a living cell using an atomic force microscope with a nanoneedle. *Nano. Lett.* 5**,** 27-30.

Oliver W, Pharr G (1992) An improved technique for determining hardness and elastic modulus using load and displacement sensing indentation experiments, *J. Mater. Res*. 7**:** 1564-1583.

Oyen M, Cook R (2003) Load-displacement behavior during sharp indentation of viscous-elastic-plastic materials. *J. Mater. Res.* 18**:** 139-150.

Oyen ML, Cook RF (2009) A practical guide for the analysis of nanoindentation data, *J. Mech. Behav. Biomed.* 2: 396-407.

Oyen M, Ko C (2007) Examination of local variations in viscous, elastic, and plastic indentation responses in healing bone. *J. Mater. Sci.-Mater. M.* 18**:** 623-628.

Patil A, Sippel J, Martin G *et al.* (2004) Enhanced functionality of nanotube atomic force microscopy tips by polymer coating. *Nano. Lett.* 4**:** 303-308.

Proksch E, Brandner JM, Jensen JM (2008) The skin: an indispensable barrier. *Exp. Dermatol.* 17: 1063-1072.

Radmacher M (1997) Measuring the elastic properties of biological samples with the AFM. *IEEE Eng. Med. Biol.* 16**:** 47-57.

Rawlings AV, Harding CR (2004) Moisturization and skin barrier function. *Dermatol. Ther.* 17 Suppl 1: 43-48.

Roduit C, Sekatski S, Dietler G *et al.* (2009) Stiffness tomography by atomic force microscopy. *Biophys. J.* 97: 674–677.

Sader J (1998) Frequency response of cantilever beams immersed in viscous fluids with applications to the atomic force microscope. *J. Appl. Phys.* 84: 64-76.

Sader J, Chon J, Mulvaney P (1999) Calibration of rectangular atomic force microscope cantilevers. *Rev. Sci. Instrum.* 70: 3967.

Tai K, Dao M, Suresh S *et al.* (2007) Nanoscale heterogeneity promotes energy dissipation in bone. *Nature Materials* 6: 454 - 462.

Vakarelski I, Brown S, Higashitani K *et al.* (2007) Penetration of living cell membranes with fortified carbon nanotube tips. *Langmuir* 23**:** 10893-10896.

Weisenhorn A, Khorsandi M, Kasas S, *et al.* (1993) Deformation and height anomaly of soft surfaces studied with an AFM. *Nanotechnology,* 4: 106.

Yuan Y, Verma R (2006) Measuring microelastic properties of the stratum corneum, *Colloids and Surfaces B*: *Biointerfaces* 48: 6-12.

Figure Legends

Figure 1: **Testing intracellular mechanics with nanoneedles.** (a) Electron microscopy image of a nanoneedle grown on AFM tips (scale bars = 200 nm). (b) Nanostructure of part of a corneocyte from SC observed by cryo-electron microscopy of vitreous sections of human skin (scale bar of main figure = 50 nm). The cornified envelope at the interface between the extracellular lipids, seen at the bottom of the figure, and the intracellular keratin appears as a darker, electron-rich zone. The inset on the left illustrates the intracellular keratin filaments (scale bar = 15 nm), while that on the right shows another, broader cornified envelope present in a different corneocyte (scale bar = 50 nm). (c) Schematic representation of the progressive penetration of nanoneedles on AFM probes into a monolayer of corneocytes.

Figure 2: **Indentation with a nanoneedle creates a pore on the corneocyte surface.** Pseudo-3D AFM image of part of a corneocyte surface (a) before, and (b) after indentation with a nanoneedle probe of 40 nm diameter; a clear indent on the cell surface is apparent. The area imaged is 1.0 x 0.5 μm^2. (c) Vertical indentation profiles before and after the indentation. The profiles are taken along the dashed lines shown in images (a) and (b).

Figure 3: **Indentation curves from different corneocytes show a common trend. (**a) Examples of loading curves recorded from the corneocytes of a 25 year old subject; the datasets have been offset vertically for the purpose of clarity. The curves show characteristic responses of a number of different corneocytes. The inset is a histogram of penetration forces for the different corneocytes examined. (b) A set of indentation curves measured from another 25 year old subject; the dataset has again been offset for clarity. The inset shows loading curves for two subjects aged 25 and 54 years, respectively.

Figure 4: **Analysis of indentation loops allows inelastic deformation to be determined.** (a) Example of loading and unloading force curves recorded during indentation of a corneocyte using a nanoneedle probe. **(**b) Inelastic deformation calculated from indents on cells as a function of applied indentation force for two different nanoneedle diameters. A rapid change in deformation occurs at 100-200 nm, possibly due to yielding of the internal corneocyte structure. Inset shows

examples of approach curves for the two needles employed. (c) Inelastic deformation scaled to nanoneedle diameter, demonstrating a common trend. Inset images are scanning electron micrographs of the two nanoneedles used in these experiments, with diameters of 40 (top) and 75 nm (bottom).

Figure 5: **Corneocytes have a softer surface layer.** (a) Agreement of models used to calculate the reduced elastic modulus of corneocyte material from a single subject as a function of inelastic deformation. (b) Compilation of calculated reduced elastic moduli using the Oliver-Pharr model (excluding retract curve extremities) for 4 "young" volunteers (19-28 years). Data from different volunteers are distinguished by the different symbols used. Error bars express the uncertainty of the fit to the Oliver-Pharr model. Dashed lines are guides for the eye.

Figure 1

(a)

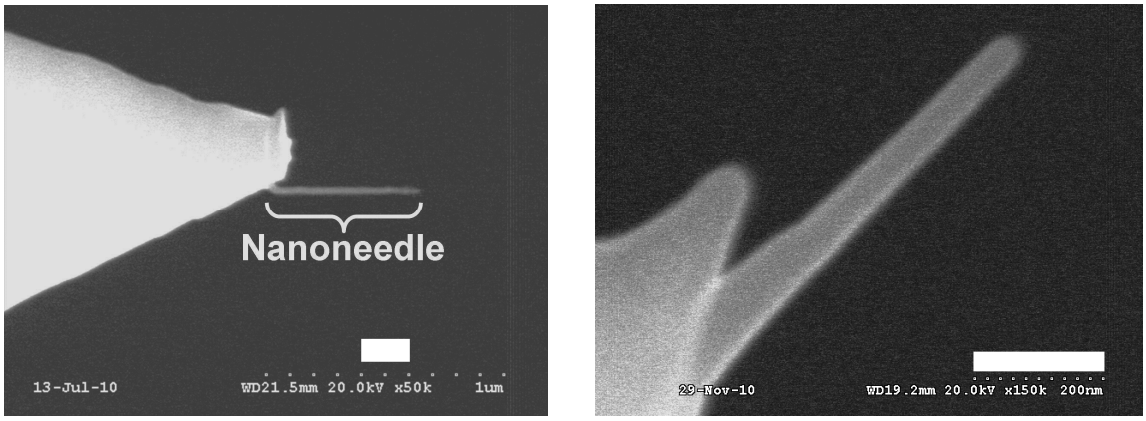

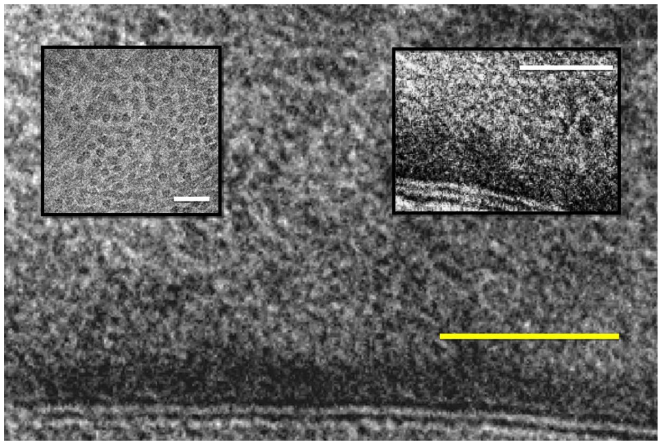

(b)

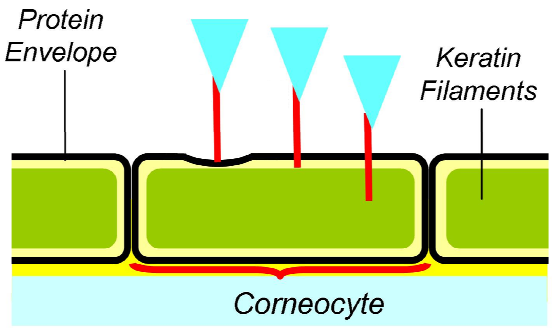

(c)

Testing intracellular mechanics with nanoneedles. (a) Electron microscopy image of a nanoneedle grown on AFM tips (scale bars = 200 nm). (b) Nanostructure of part of a corneocyte from SC observed by cryo-electron microscopy of vitreous sections of human skin (scale bar of main figure = 50 nm). The cornified envelope at the interface between the extracellular lipids, seen at the bottom of the figure, and the intracellular keratin appears as a darker, electron-rich zone. The inset on the left illustrates the intracellular keratin filaments (scale bar = 15 nm), while that on the right shows another, broader cornified envelope present in a different corneocyte (scale bar = 50 nm). (c) Schematic representation of the progressive penetration of nanoneedles on AFM probes into a monolayer of corneocytes.

Figure 2

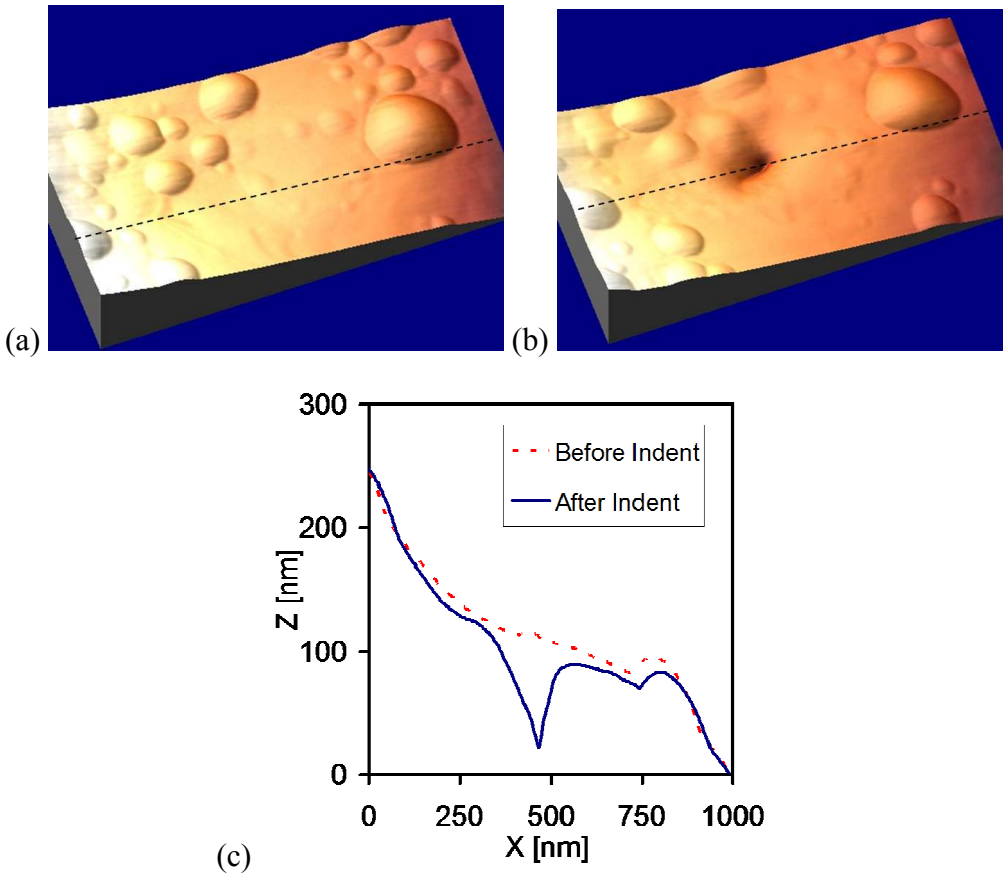

Indentation with a nanoneedle creates a pore on the corneocyte surface. Pseudo-3D AFM image of part of a corneocyte surface (a) before, and (b) after indentation with a nanoneedle probe of 40 nm diameter; a clear indent on the cell surface is apparent. The area imaged is 1.0 x 0.5 μm^2. (c) Vertical indentation profiles before and after the indentation. The profiles are taken along the dashed lines shown in images (a) and (b).

Figure 3

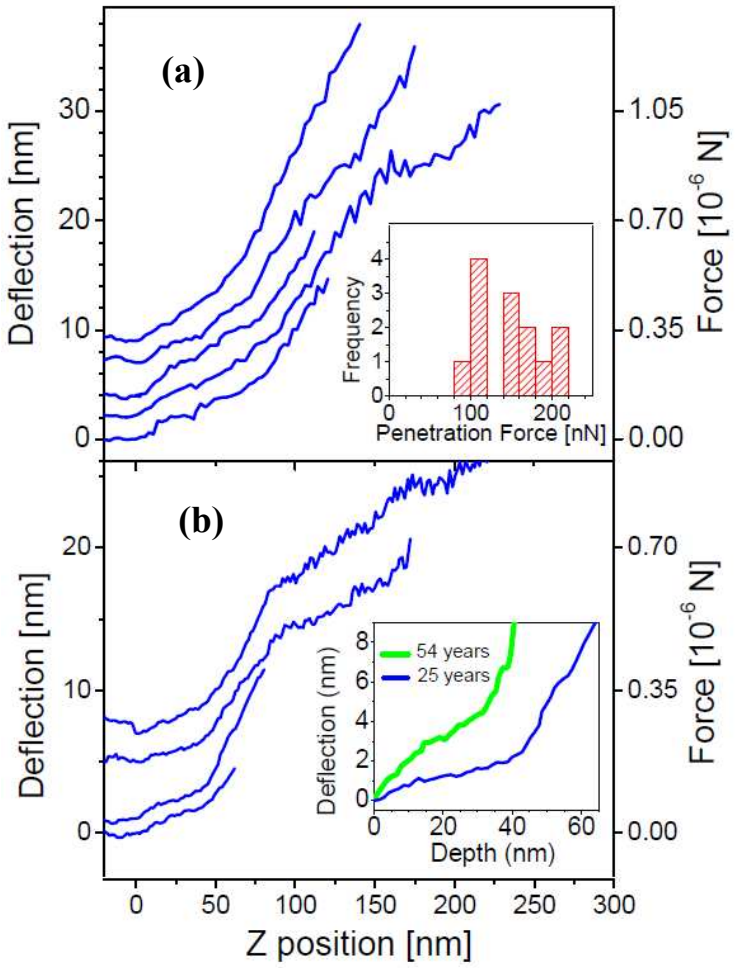

Indentation curves from different corneocytes show a common trend. (a) Examples of loading curves recorded from the corneocytes of a 25 year old subject; the datasets have been offset vertically for the purpose of clarity. The curves show characteristic responses of a number of different corneocytes. The inset is a histogram of penetration forces for the different corneocytes examined. (b) A set of indentation curves measured from another 25 year old subject; the dataset has again been offset for clarity. The inset shows loading curves for two subjects aged 25 and 54 years, respectively.

Figure 4

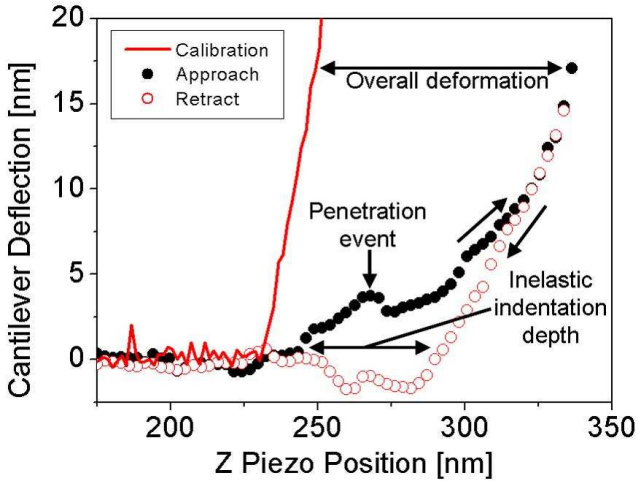

(a)

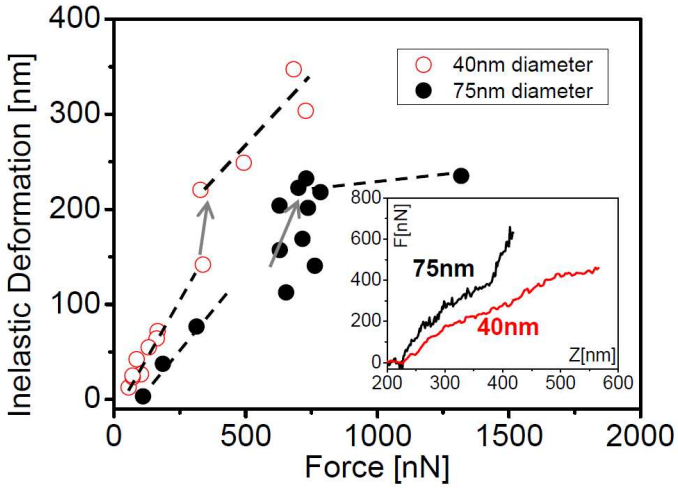

(b)

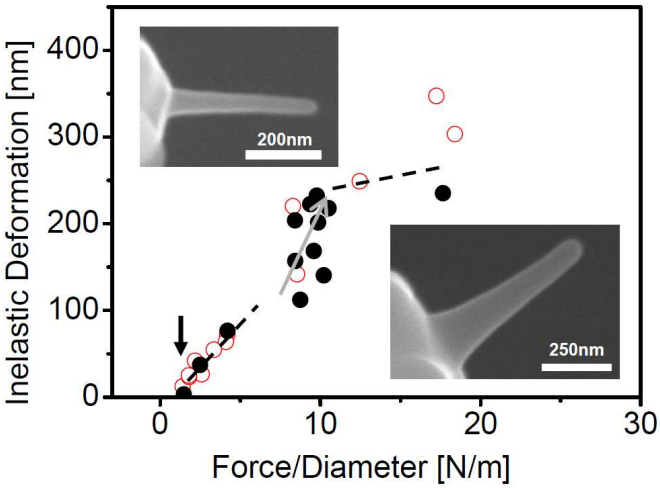

(c)

Analysis of indentation loops allows inelastic deformation to be determined. (a) Example of loading and unloading force curves recorded during indentation of a corneocyte using a nanoneedle probe. (b) Inelastic deformation calculated from indents on cells as a

function of applied indentation force for two different nanoneedle diameters. A rapid change in deformation occurs at 100-200 nm, possibly due to yielding of the internal corneocyte structure. Inset shows examples of approach curves for the two needles employed. (c) Inelastic deformation scaled to nanoneedle diameter, demonstrating a common trend. Inset images are scanning electron micrographs of the two nanoneedles used in these experiments, with diameters of 40 (top) and 75 nm (bottom).

Figure 5

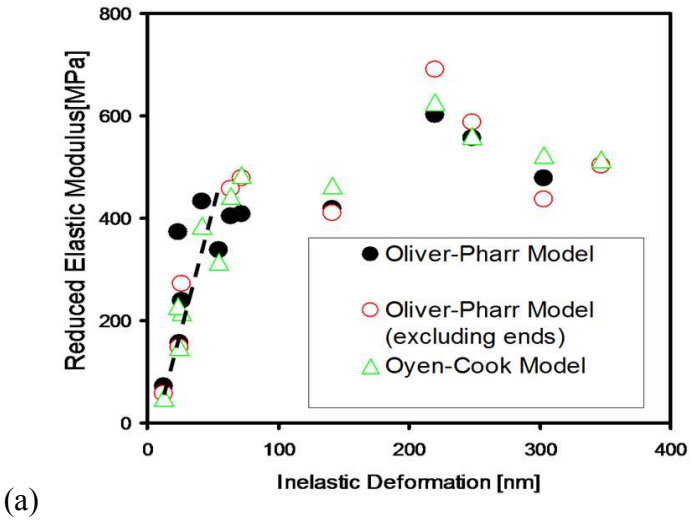

(a)

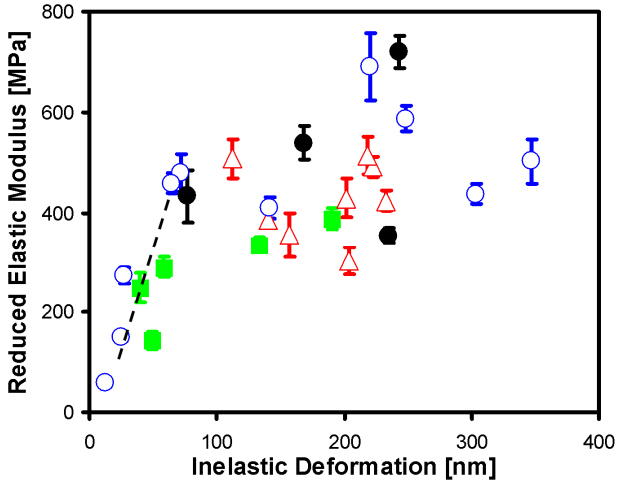

(b)

Corneocytes have a softer surface layer. (a) Agreement of models used to calculate the reduced elastic modulus of corneocyte material from a single subject as a function of inelastic deformation. (b) Compilation of calculated reduced elastic moduli using the Oliver-Pharr model (excluding retract curve extremities) for 4 "young" volunteers (19-28 years). Data from different volunteers are distinguished by the different symbols used. Error bars express the uncertainty of the fit to the Oliver-Pharr model. Solid lines are guides for the eye.